

ARTIFICIAL MAGNETIC MATERIALS BASED ON THE NEW MAGNETIC PARTICLE: METASOLENOID

S. Maslovski, P. Ikonen, I. Kolmakov, and S. Tretyakov

Radio Laboratory/SMARAD
Helsinki University of Technology
P.O. Box 3000, FI-02015 HUT, Finland

M. Kaunisto

VTT Technical Research Center of Finland
P.O. Box 1200, FI-02044 VTT, Finland

Abstract—New possibilities to design artificial magnetic materials for microwave frequencies are considered. Such composites can be used in microwave engineering at frequencies where no natural low-loss magnetic materials are available. A new magnetic particle (*metasolenoid*) formed by a stack of many parallel and very closely spaced single broken loops is proposed and analyzed analytically, numerically, and experimentally. It is shown that the effective permeability can reach reasonably high values over a wide frequency range when using such inclusions.

1 Introduction

2 Analytical Modeling

- 2.1 The Operational Principle
- 2.2 Metasolenoid
- 2.3 Material Parameters
- 2.4 Numerical Example

3 Numerical Modeling in HFSS

- 3.1 Metasolenoid
- 3.2 Arrays of Separate MSSR
- 3.3 Arrays of Swiss Rolls

4 Experimental Verification

4.1 Measured Results

5 Conclusions

Acknowledgment

References

1. INTRODUCTION

Many engineering problems of antenna and microwave techniques could find elegant solutions with the use of low-loss and broadband magnetic materials. Despite the progress in the manufacturing technology of ferrite materials (barium-hexaferrite-based composites were reported [1] that are operational at frequencies up to 500 MHz), we still have to deal with the well-known fact that the natural magnetic materials lose their magnetic properties at microwave and millimeter-wave frequencies. This means that at high frequencies magnetics have to be realized as composite materials with conducting inclusions of complex shapes (split-ring-based structures were reported [2] that are active even in the infrared).

To maximize the effect of artificial magnetism, the inclusions are usually designed so that the current excited in the inclusions forms loops. It can be shown that the total impedance determining the induced current at the frequencies lower than the inclusion resonance must be capacitive in order to realize artificial paramagnetics (e.g., [3, 4]). In this case the inclusion magnetic moment is in phase with the applied magnetic field and the composite behaves as a magnetic with the effective relative permeability greater than unity. Various practical designs such as broken loops [5] and pairs of broken loops [6] utilize air gaps in conducting rings forming the particles to achieve capacitive loading. The load capacitance can be increased by using bulk capacitances of various types [3, 7]. Artificial magnetism exists in chiral and bi-anisotropic composites [8, 9] where the inclusions have spiral shapes. Chirality can be compensated using the system of two coupled spirals of the opposite handedness [10].

More recently, the split-ring resonator (SRR) shape was proposed [11], where the two rings are very strongly capacitively coupled. Capacitive coupling may be even more increased in so-called modified split-ring resonators (MSRR) [12]. At HF and possibly VHF frequencies, so called “Swiss rolls” — rolled metal sheets — have strong magnetic properties [11], but these structures are electrically conducting along the rolls axes. This, in addition to the restricted

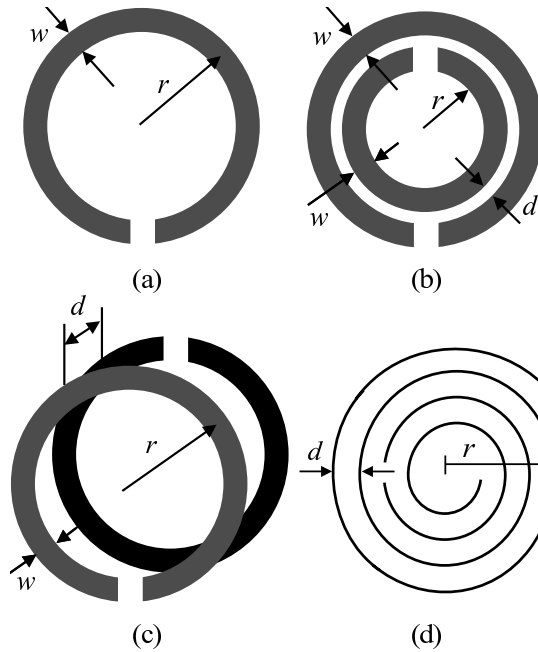


Figure 1. (a) Single split-ring resonator. (b) Split-ring resonator (SRR). (c) Modified split-ring resonator (MSRR) (d) Cross section of the Swiss roll.

operational frequency, limits their potential applications. Some of the known geometries are illustrated in Figure 1. The main drawback of all these designs is that the effective magnetism quickly vanishes when the frequency deviates from the particle resonance. Note that near the resonance the real part of the effective permeability can be negative if the quality factor of the resonator is enough high.

As a possible solution to this problem, we introduce a stack made from single broken loops (Figure 2, left). We call it *metasolenoid*. As is seen from the figure the loops are of rectangular shape. Such a shape is chosen to increase packing density when many metasolenoids are put together to form a medium. Alternatively, this solution can be considered and realized as a Swiss roll cut into many individual parallel rolls, see Figure 2, right (other geometries of loops are possible as well). When single loops or strip spirals are placed in a dense stack, the magnetic flux is very much concentrated inside the structure and it is directed along the particle axis. Because of this, the particle very strongly responds to external magnetic fields, similarly to the known Swiss roll. On the other hand, the structure is not conducting along

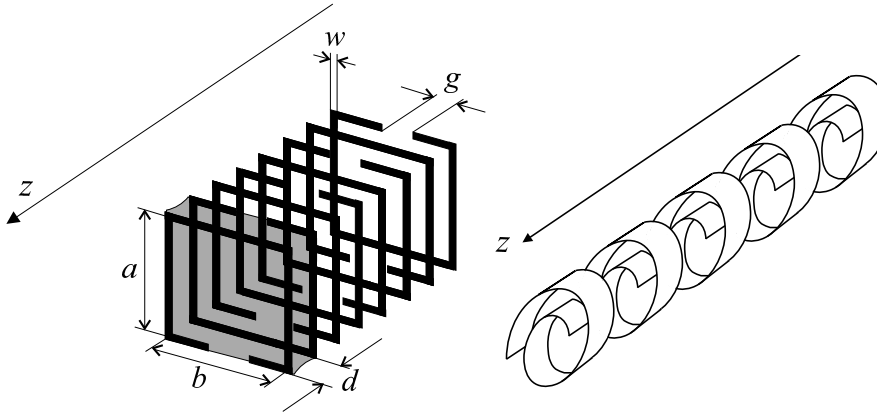


Figure 2. Two examples of alternative geometries of the metasolenoid.

the axis and it can be operational at the microwave and millimeter wave frequencies, which are important advantages as compared with the Swiss roll. The bandwidth of this new particle does not itself widen (when losses in the metal dominate over the radiation losses). However, we obtain high values of the effective permeability over a noticeably wider range of frequencies *far away from the resonance* as compared to the case of SRR or MSRR composites.

In a finite sample of a medium made of metasolenoids the neighboring solenoids interact because the flux escaping from the end of one metasolenoid penetrates into another one. Such interaction was thoroughly investigated in [13] and also mentioned in [14] for a slab made of swiss-rolls. It was found that at frequencies below the resonance the role of interaction is much less significant than for the frequencies just above the resonance where certain complicated wave patterns can be observed. Because in the present paper we do not study such interactions, our results are applicable either when the metasolenoids are in such conditions that they can be considered as effectively infinite or when the operational frequency is well below the metasolenoid resonance, where magnetization is distributed uniformly even in finite-sized stacks of metasolenoids.

2. ANALYTICAL MODELING

As discussed in the introduction, there are several types of magnetic inclusions known from the literature. Some of them are presented in Figure 1. Basically, the operation principle of all these inclusions is the same. We will review it shortly in the next subsection. After that

we will introduce our own design: a stack composed of single split-ring resonators or other kinds of capacitively loaded loops (a *metasolenoid*) and present a more detailed analytical model for this new inclusion.

2.1. The Operational Principle

We assume that particles shown in Figure 1 are excited by an external magnetic field orthogonal to the picture plane. The magnetic field induces electromotive forces in the inclusions. For cases (b) and (c) there are actually two conducting rings, and in case (d) there is one or several turns of a conducting sheet in a particle. Nevertheless, near the lowest resonant frequency all these structures can be described by means of the total effective current circulating around the inclusions.

The circulating total current flows across the capacitive gaps introduced in the structures and creates magnetic field which results in an inductive part of the total impedance of an inclusion. Finite metal conductivity and magnetic dipole radiation contribute to the real part of the total impedance. Hence, the effective induced current for all the structures shown in Figure 1 can be expressed as

$$I = \frac{\mathcal{E}^{\text{ext}}}{Z_{\text{tot}}} = \frac{\mathcal{E}^{\text{ext}}}{j\omega L_{\text{eff}} + \frac{1}{j\omega C_{\text{eff}}} + R_{\text{eff}}} \quad (1)$$

The formulas for the effective circuit parameters L_{eff} , C_{eff} , and R_{eff} can be found in [5, 6, 11, 12]. From (1) we see that the particles exhibit resonant responses. At the frequencies lower than the resonant frequency the capacitive part of the total impedance Z_{tot} dominates. Next, the external electromotive force \mathcal{E}^{ext} can be found as

$$\mathcal{E}^{\text{ext}} = -j\omega\mu_0 N S H^{\text{ext}} \quad (2)$$

where N is the number of turns [$N = 1$ for the cases (a), (b), and (c)], and S is the inclusion cross-section area penetrated by the external magnetic field H^{ext} . The magnetic moment induced in a particle is

$$m = \mu_0 N S I = \frac{\omega^2 \mu_0^2 N^2 S^2 C_{\text{eff}} H^{\text{ext}}}{1 - \omega^2 L_{\text{eff}} C_{\text{eff}} + j\omega R_{\text{eff}} C_{\text{eff}}} \quad (3)$$

At low frequencies the magnetic moment is proportional to the effective capacitance. One of the goals of our design will be to increase this capacitance as much as possible.

2.2. Metasolenoid

The geometry of the proposed artificial particle which we call *metasolenoid* is shown in Figure 2. With different geometries of the capacitively loaded loops (two variants are illustrated by Figure 2), the operational principle is basically the same. The structure with split rings has less pronounced bi-anisotropy due to its higher symmetry, and a possible advantage of a lower inductance of the loops. For this reason, we will consider the particle operation for the geometry shown on the left-hand side of Figure 2.

In the following derivation we assume the structure to be infinite in the z direction. The external magnetic field is applied along the z axis and is uniform inside the metasolenoid. Let us consider the volume between two neighboring split rings (the shaded volume in Figure 2). The external magnetic field induces currents on the surfaces of the rings. Two currents flow at the two ring surfaces which are internal to the shaded volume. Because of the strong capacitive coupling of the broken rings the current from one surface of the first ring flows to the second ring crossing two capacitive gaps on the way, like in a usual MSRR [12]. The sum the two currents induced on the internal surfaces of two neighboring rings represents the effective current circulating in a cell of the metasolenoid. Similarly to the MSRR case, such current is effectively uniform around the solenoid. We denote it as I .

In our design, the rings are packed rather densely, that is, the distance between the loop planes d is much smaller than the cross section dimensions a, b (Figure 2). Thus, for the infinite metasolenoid we can assume that all the magnetic flux is concentrated inside the metasolenoid volume, which means that the flux is uniform along the z axis. Under these assumptions, the total magnetic flux in the metasolenoid can be expressed as

$$\Phi = \mu_0 S H^{\text{ext}} + \frac{\mu_0 S I}{d} \quad (4)$$

where $S = ab$ is the cross-section area of the metasolenoid; a, b, d are defined in Figure 2. In this formula, the first term is the flux induced by the external magnetic field H^{ext} . In the second term, I/d is the current density on the metasolenoid surface that is equal to the magnetic field inside the metasolenoid generated by the cell currents I . The flux is calculated simply by multiplying this value by the area S and the free-space permeability.

The electromotive force produced by the total flux must be equal to the total voltage drop on the capacitive gaps and the effective loss

resistance:

$$-j\omega\Phi = I \left(\frac{1}{j\omega C_{\text{eff}}} + R_{\text{eff}} \right) \quad (5)$$

Here C_{eff} is the total capacitance of two capacitive gaps connected in series. The effective capacitance can be found by the following approach. In an infinite metasolenoid, equipotential surfaces are formed between every pair of rings due to the symmetry. Therefore, the formula for the capacitance per unit length C_0 of a symmetric strip line [15] can be used:

$$\frac{C_0}{\varepsilon_r \varepsilon_0} = 4 \frac{K(k)}{K'(k)}, \quad k = \tanh \frac{\pi w}{2d} \quad (6)$$

where w is the strip width, ε_r is the relative permittivity of the material which supports the rings, $K(k)$ and $K'(k)$ are elliptic integrals, see [15] for the definition. Taking into account the symmetry considerations and the series connection of two capacitive gaps, the effective capacitance reads

$$C_{\text{eff}} = \frac{C_0 l}{16} = \frac{\varepsilon_r \varepsilon_0 l}{4} \frac{K(k)}{K'(k)} \quad (7)$$

where $l = 2(a+b-g)$ is the total overlapping length of two neighboring rings, see Figure 2. The effective resistance R_{eff} is the sum of the radiation resistance and the loss resistance. Combining (4) and (5) we have

$$-\frac{j\omega\mu_0 S H^{\text{ext}}}{I} = \frac{j\omega\mu_0 S}{d} + \frac{1}{j\omega C_{\text{eff}}} + R_{\text{eff}} \quad (8)$$

From here we see that we can define the effective inductance of the metasolenoid as

$$L_{\text{eff}} = \frac{\mu_0 S}{d} \quad (9)$$

Finally, the total impedance of the metasolenoid is

$$Z_{\text{tot}} = j\omega L_{\text{eff}} + \frac{1}{j\omega C_{\text{eff}}} + R_{\text{eff}} \quad (10)$$

2.3. Material Parameters

Let us estimate the effective permeability of a medium densely filled with many parallel metasolenoids. For the case of magnetic excitation $\mathbf{H}^{\text{ext}} = H^{\text{ext}} \mathbf{z}_0$ (see Figure 2) we can write for the magnetic flux density in the metasolenoid

$$\mathbf{B}_{\text{sol}} = \mu_0 \mathbf{H}^{\text{ext}} + \mathbf{M}_{\text{sol}} \quad (11)$$

where $\mathbf{M}_{\text{sol}} = M_{\text{sol}}\mathbf{z}_0$ is the magnetic moment per unit volume of the metasolenoid. The amplitude of \mathbf{M}_{sol} reads

$$M_{\text{sol}} = \frac{\mu_0 I}{d} = -\frac{j\omega\mu_0^2 S H^{\text{ext}}}{Z_{\text{tot}} d} \quad (12)$$

In a medium filled by infinite metasolenoids oriented along the z axis the average magnetic induction is

$$\mathbf{B} = \mu_0 \mathbf{H}_{\text{ext}} + \mathbf{M}_{\text{sol}} V_r \quad (13)$$

where V_r is the volume filling ratio. Finally, the effective relative permeability of the medium can be found as

$$\mu_{\text{eff}} = 1 - V_r \frac{j\omega\mu_0 S}{Z_{\text{tot}} d} \quad (14)$$

In the measurements we will use a finite-size segment of a metasolenoid. The magnetic polarizability of the sample depends on its shape. To take into account this influence we approximate the sample shape by an ellipsoid (Figure 3). Utilizing the known formula for the polarizability of the ellipsoid (e.g., [16]) we can write for the magnetic polarizability of the metasolenoid

$$\alpha_{\text{mm}} = \frac{\mu_0 \pi}{6} \frac{abh(\mu_{\text{eff}} - 1)}{1 + N_z(\mu_{\text{eff}} - 1)} \quad (15)$$

where h is the longitudinal length of the metasolenoid and N_z is the depolarization factor along the longitudinal axis. In this case we should let $V_r = 1$ in (14).

2.4. Numerical Example

In this example we analyze a metasolenoid with the parameters given in Table 1. The notations refer to Figure 2. The quantity ε_r also given there is the permittivity of the laminate on top of which the metasolenoid split rings are printed. The loss tangent of this material equals $\tan \delta = 0.002$.

Table 1. The parameters of the metasolenoid sample.

a mm	b mm	w mm	g mm	d mm	ε_r
3.5	3.5	0.4	1.0	0.127	2.2

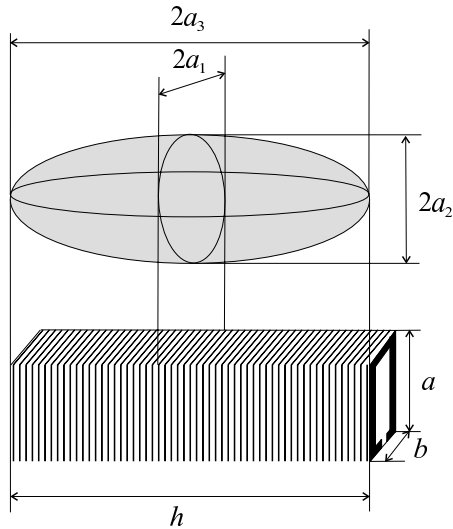


Figure 3. A metasolenoid segment approximated by an ellipsoid.

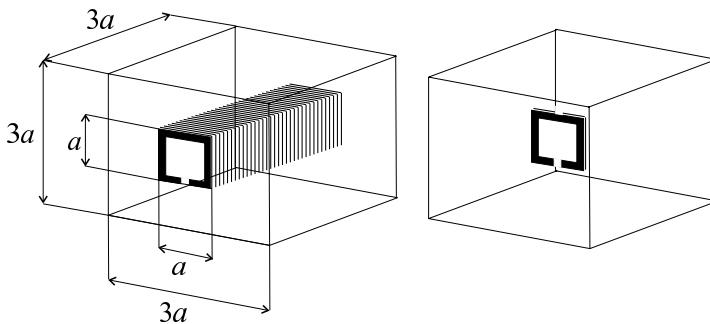


Figure 4. Unit cells occupied by a metasolenoid and a MSRR.

To compare the magnetic response of media filled by metasolenoids and by usual MSRR particles we do the following. We choose a specific unit cell size and place exactly one particle in a unit cell, see Figure 4. In case of the MSSR medium the particles form a cubic lattice with a small period as compared to the wavelength (both in the medium and in free space). The distance between the rings forming the MSRR particles has been decreased by a factor $1/22.5$ compared to the distance between the rings of a reference metasolenoid. Due to this the particles resonate at the same frequency still maintaining the same cross-section area. All the other dimensions are as in Table 1.

To calculate the effective relative permeability of the MSRR medium, we utilize the known Clausius-Mossotti relation:

$$\mu_{\text{eff}} = 1 + \frac{n\alpha_{\text{mm}}}{\mu_0 - \frac{n\alpha_{\text{mm}}}{3}} \quad (16)$$

where the volume concentration is $n = 1/(3a)^3$ in our case. The magnetic polarizability α_{mm} of the MSRR can be calculated using formulas available from the literature [12].

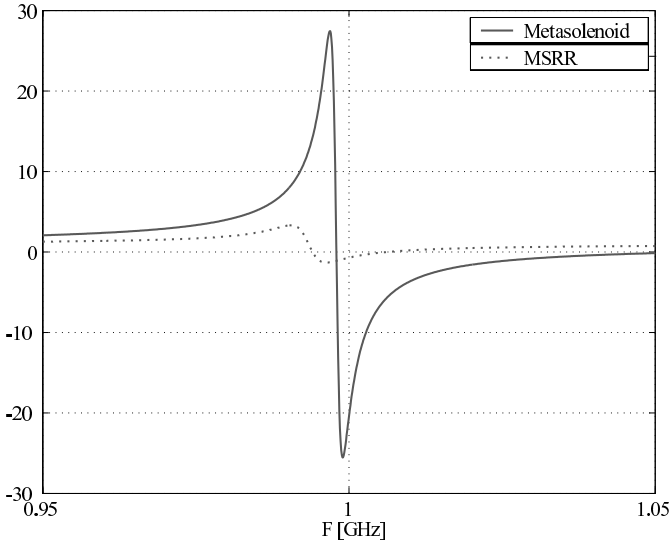


Figure 5. The real part of μ_{eff} for a metasolenoid medium (the solid curve) and an MSRR medium (the dashed curve) as functions of frequency.

The metasolenoid medium in our example is formed by a set of infinite and parallel metasolenoids with square loops of side a and the distance between the metasolenoids $3a$. For the analysis we consider the whole infinite structure as a set of “unit cells” of size $3a \times 3a \times 3a$ shown in Figure 4, left. To calculate the effective permeability for this medium filled with metasolenoids, we use formula (14). The volume fraction $V_r = 1/9$. Figure 5 compares the permeabilities of the metasolenoid medium and the MSRR medium with the same dimensions of the loops and of the unit cell.

As the unit cell sizes decrease towards the value of a , the dispersion curve of the MSRR composite approaches that for the metasolenoid medium (calculated for the same decreased cell size). This can

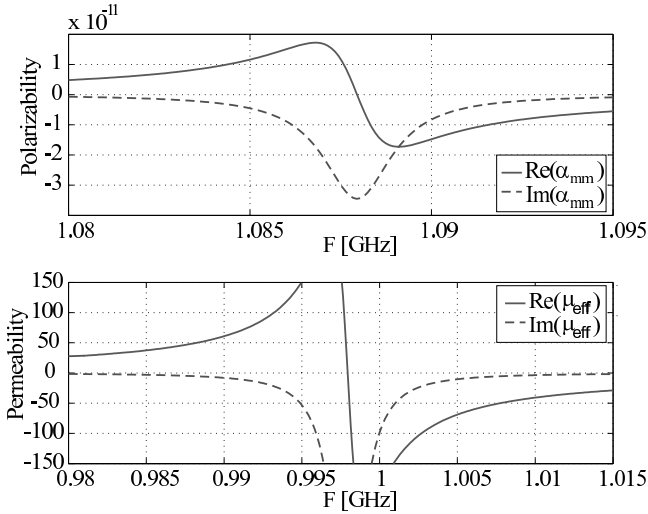


Figure 6. The polarizability α_{mm} (top) and the permeability μ_{eff} (bottom): analytical model.

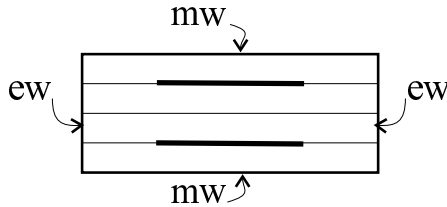


Figure 7. Definition of the simulation box. “ew” denotes electric walls, “mw” denotes magnetic walls. The rings are seen as bold lines (side view).

be understood when thinking how the magnetic flux penetrates the particles in these two cases. If the unit cell is large compared to the size of an MSRR, the flux lines penetrate the rings but also form loops closing around the edges of the particles. The metasolenoid structure effectively prevents the flux from escaping outside the solenoid, thus, a noticeable difference is expected in the curves. Figure 6 shows the dispersion curve for the polarizability and the relative permeability of the metasolenoid in the case when a medium is densely filled with metasolenoids, such that V_r approaches unity.

3. NUMERICAL MODELING IN HFSS

Because the dimensions of split rings in MSRRs or the metasolenoid are small: $a \simeq 0.1\lambda$, it is impractical to model effectively a real-size sample of a metamaterial based on such inclusions. Instead, an infinite medium can be modeled by placing a finite number (two split rings are usually enough) of particles in a box with suitable boundary conditions at the box walls. This has been done with a simulation setup shown in Figure 7. Simulations are performed so that electric walls (denoted as ew) are on the right and the left sides of the box, and magnetic walls (mw) are on the top and the bottom sides of the box. The broken rings are seen as lines there because the line of sight is parallel to the ring planes. Two ports are at the front and at the back walls of the box, with the port voltages measured between the two electric walls of the structure. The boundary conditions simulate a plane-wave excitation and, with a certain degree of accuracy, the periodicity of the magnetic and electric field distributions in the structure. To take into account the periodicity of the metasolenoid exactly, one must use either true periodical boundary conditions, or combined electric wall/magnetic wall conditions where the magnetic walls pass through the middle plane of the metal rings of a small but finite thickness. In the last case, the image current on the “outside” surface of the ring is the same as that on the internal surface. We have used both configurations (that shown in Figure 7 and the other with magnetic walls passing through metal rings of thickness 0.002 mm), with very close results in both cases.

A dielectric material with $\epsilon_r = 7.8$, $\tan \delta = 0.002$ (typical for LTCC technology processes) was chosen as the matrix medium. The split rings were designed for the resonant frequency near 10 GHz.

3.1. Metasolenoid

A set of split rings ($w = 0.2$ mm, $g = 0.2$ mm and $a = b = 1.2$ mm) with the distance between the loops $d = 0.41$ mm has been simulated. In this case the total height of the dielectric box in the simulations is $h = 2d = 0.82$ mm. The structure has a strong resonant response with a reflection zero approximately at 9 GHz and a transmission minimum slightly above 10 GHz (see Figure 8). These effects can be explained as following. The reflection coefficient vanishes when the simulated waveguide segment is matched with the incidence port. This happens when the effective impedance of the simulated metasolenoid medium layer approaches the characteristic impedance of the same waveguide, but without the metasolenoid. The metasolenoid has a certain electric polarizability, and this polarizability dominates over the magnetic polarizability at the frequencies significantly lower than

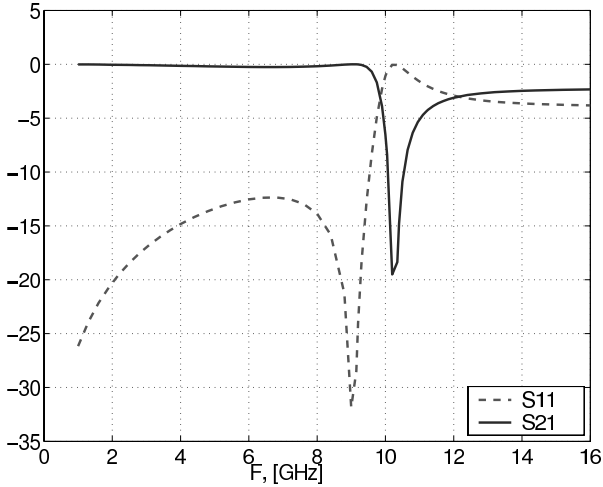


Figure 8. The frequency response of a simulated metasolenoid. The solid line and the dashed lines represent the magnitude of S_{21} and S_{11} , respectively.

the resonant frequency. When the frequency increases, the magnetic polarizability of the metasolenoids increases. At the frequencies around the resonant frequency the magnetic polarizability dominates. Hence, there is such a frequency below the resonance at which the effective medium magnetic response is balanced with the effective medium electric response providing the effective impedance of the metasolenoid layer equal to the the characteristic impedance of an empty waveguide. We observe a reflection zero at this frequency.

The transmission coefficient minimum corresponds to the frequency range where the effective magnetic permittivity of the medium is negative. In this range there are only decaying solutions for the modes in the structure. The field distributions have been analyzed also. It was found that at the resonance the magnetic field is indeed strongly concentrated inside the metasolenoid. Strong electric field is excited in between the overlapping areas of neighboring rings.

3.2. Arrays of Separate MSSR

The effect of the varying distance between pairs of rings in a metasolenoid has been investigated. The simulation environment is illustrated in Figure 9. Choosing the value of d , we can regulate the distance between the single pairs. When this distance is not equal to Δ and is increased, a metasolenoid transforms to a linear array of

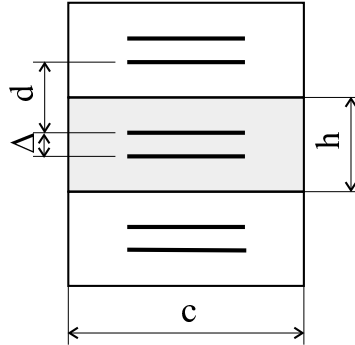


Figure 9. Definition of the simulation box for arrays of separate MSSR. As for the metasolenoid (Figure 7), the box containing only one pair of rings is bounded by magnetic walls on the top and bottom and by electric walls on the two sides. The rings are seen as bold lines (side view).

separate MSRRs. Distances $d = 0.82$ mm and $d = 2.87$ mm have been used in the simulations. Simulated data are presented in Figure 10. The structure with $d = 0.41$ mm has been simulated on an improved mesh (the previous simulation was done with default mesh settings), which shifts down the resonant frequency to 1.2 GHz (13 percent). The distribution of magnetic field in the case of separate MSSR forming an array is different from the metasolenoid case. It has been observed that the magnetic flux is circulating around the edges of MSRRs and the flux concentration effect is significantly lower than in the case of a metasolenoid.

3.3. Arrays of Swiss Rolls

Swiss rolls are formed by rolled continuous metal sheets [see Figure 1(c)]. The particular shape of the cross-section of such rolls is not relevant, so for the sake of comparison with the metasolenoid we consider the cross section shown in Figure 11, left. The structures with similar cross-section dimensions ($d_1 = 1.2$ mm, $d_2 = 0.4$ mm, $g = 0.4$ mm) have been simulated. Calculated S -parameters are presented on Figure 12. By inspecting these curves and the magnetic field distribution it is clear that Swiss rolls possess a similar behavior to that of metasolenoids. The longitudinal conductivity of the Swiss rolls does not matter in the present simulation conditions because the external electric field is orthogonal to the axes of the Swiss rolls. Let us note again that with MSRRs the flux lines are circulating around

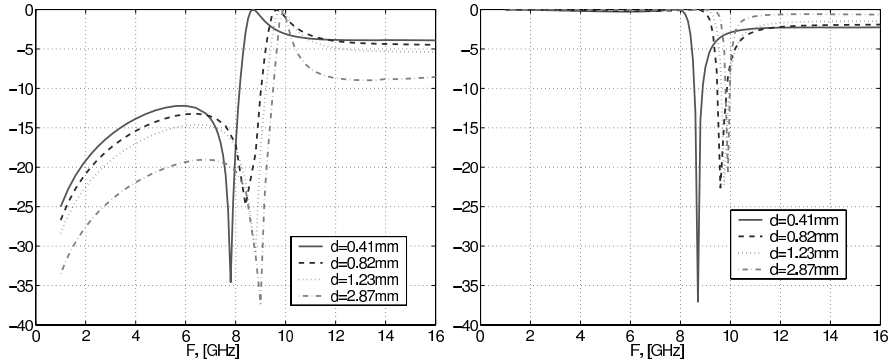


Figure 10. Results of HFSS simulations for the case of separate MSRR forming an artificial crystal. The S_{11} magnitude plot is given on the left and the S_{21} magnitude is on the right. The several curves on each plot correspond to different distances between the MSSRs in stacks (parameter d).

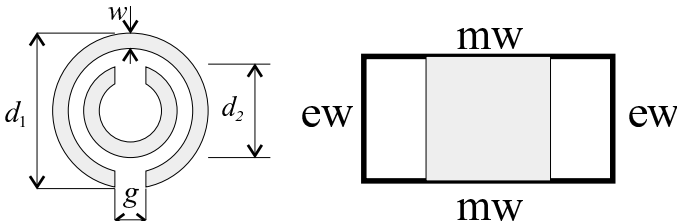


Figure 11. Definition of the simulation box for the Swiss roll medium. The notations are the same as in Figure 7.

the particle edges whereas in the cases of metasolenoids and Swiss rolls the structures efficiently prevent the flux lines from escaping outside the inclusion volume.

4. EXPERIMENTAL VERIFICATION

The overall dimensions of a metasolenoid segment used in waveguide reflection measurements are $6.5 \times 6.5 \times 7.6 \text{ mm}^3$. Because of a small size compared to the wavelength we approximate the metasolenoid section as a magnetic dipole and extract the polarizability from the measured results utilizing the known theory for waveguide excitation [15].

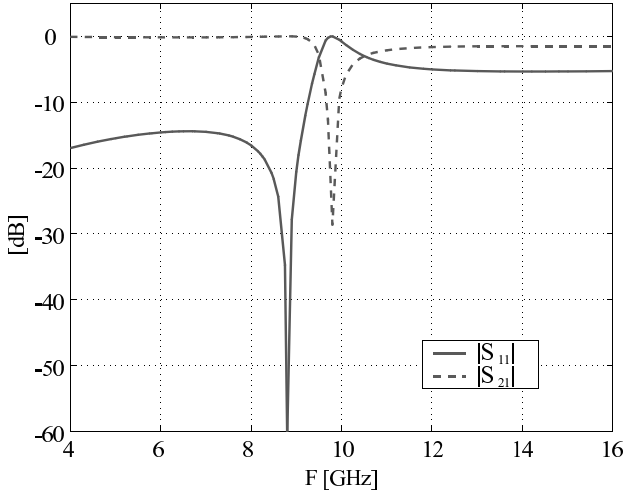


Figure 12. Simulation results for an array of Swiss rolls. The S_{11} and S_{21} magnitudes are represented by the solid curve and the dashed curve, respectively.

For the magnetic moment of the metasolenoid we can write

$$m = \alpha_{\text{mm}} H^{\text{loc}} = \alpha_{\text{mm}} (H^{\text{inc}} + H^{\text{sc}}) \quad (17)$$

where α_{mm} is the magnetic polarizability of the metasolenoid and H^{loc} is the local field exciting currents in the metasolenoid. H^{inc} is the external field and H^{sc} is the scattered field from the sample. Expressing the scattered waveguide field as a superposition of the waveguide modes, we can write for a mode of the scattered field

$$H_q^{\text{sc}} = A_q^{\pm} H_q^{\pm} = A_q^{\pm} \quad (18)$$

where signs \pm refer to two opposite propagation directions of an excited mode characterized by index q . We assume the eigenmode magnetic field H_q^{\pm} to have amplitude equal to unity. The well-known formula for the amplitude coefficient is [15]

$$A_q^{\pm} = -\frac{1}{2\kappa_q} \frac{j\omega \mathbf{m} \cdot \mathbf{H}_q^{\mp}}{\int \mathbf{H}_{q_t}^+ \cdot \mathbf{H}_{q_t}^- dS} \quad (19)$$

where the subscript t denotes the transverse field component and κ_q is the wave impedance. The integral in the denominator is over the waveguide cross-section area.

We are interested only in the main TE mode. In this case the last expression can be reduced to the following result:

$$A_{\text{TE}_{10}}^+ = \frac{\beta_{10}IS}{j sl} \quad (20)$$

where I is the induced current in the metasolenoid rings, s and l are the cross section sizes of the waveguide, β_{10} is the propagation factor of the TE₁₀ mode and S is the effective area of a single split ring. Knowing the amplitude coefficient we can solve the induced current from equation (17) and substitute this expression into (20). Because we use a matched waveguide in the measurements, we can write for the reflection coefficient:

$$A_{\text{TE}_{10}}^+ = \Gamma = \frac{\beta_{10}\alpha_{mm}}{j sl \mu_0 - \alpha_{mm} \beta_{10}} \quad (21)$$

From here we solve the unknown polarizability as a function of the measured reflection coefficient Γ :

$$\alpha_{mm} = \frac{j sl \mu_0 \Gamma}{\beta_{10}(\Gamma + 1)} \quad (22)$$

The electric dipole moment created by electric fields can be estimated as the polarizability of a metal ellipsoid of the same dimensions as our sample. The reflection from the induced electric dipole is many orders of magnitude smaller than that from the magnetic moment and can be neglected.

4.1. Measured Results

A standard one-meter long WR-650 waveguide with two transitions to coaxial cables has been used in the measurements. Figure 13 shows the measured dispersion curve for the polarizability of the metasolenoid. The measured data are presented in Table 2, second row. The measured values agree qualitatively well with the theoretical predictions, see Table 2.

Table 2. Theoretically predicted and measured parameters of the metasolenoid sample.

	f_{res} GHz	$\text{Re}\{\alpha_{\text{max}}\}$ H·m ²	$ \alpha_{\text{max}} $ H·m ²	$\mu_{\text{eff}}^{\text{max}}$
Theory and simulations	0.998 (1.12)	1.7×10^{-11}	3.3×10^{-11}	230
Measurements	1.21	1.4×10^{-11}	2.7×10^{-11}	–

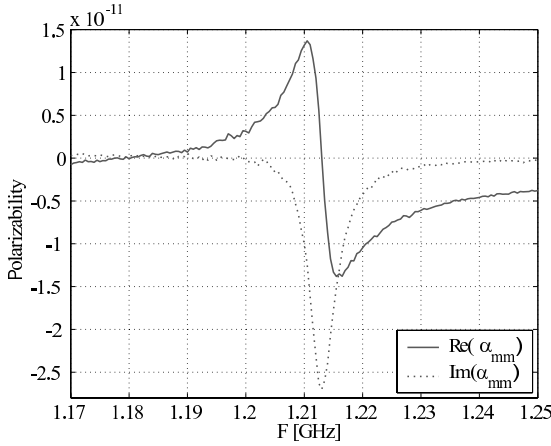


Figure 13. The real and imaginary parts of the metasolenoid polarizability α_{mm} as functions of frequency: the measured results.

5. CONCLUSIONS

In this paper, we have introduced a new magnetic particle — the metasolenoid. A simple analytical model for a new artificial magnetic inclusion has been introduced and validated by simulations and measurements. Table 2 gathers the analytically (the first row) and experimentally (the second row) obtained data. The quantity $\mu_{\text{eff}}^{\text{max}}$ corresponds to the maximum value of the real part of the effective permeability. The resonant frequency predicted by HFSS is presented in brackets (for the same particle geometry and the materials). We can point out that the real part of μ_{eff} remains high over a very wide frequency range (Figure 6) exceeding 10 still at frequencies about five percents lower than the resonant frequency of the metasolenoid.

The Swiss rolls work in the same way, however, in the Swiss roll currents can also flow parallel to the axis of the particle. If the polarization is such that the electric field is not orthogonal to the axis of the particle, the Swiss roll medium acts as an effective plasma because the current freely flows along the length of the cylinders. These problems are avoided with the metasolenoid, a fact that makes the metasolenoid more preferable in many applications, especially at microwaves. Up to our knowledge, all present Swiss roll realizations have been targeted to the radio frequencies only.

There is also a possibility to have non-uniform magnetization oscillations and slow waves of magnetization excited in a metasolenoid. We do not explore this phenomenon in the present work.

ACKNOWLEDGMENT

This work has been partially funded by the Academy of Finland and TEKES through the Center-of-Excellence program and it was coordinated with the program of the European Center of Excellence *Metamorphose*. Part of this work was presented at *Progress in Electromagnetics Research Symposium*, Pisa, Italy, March 2004 [17].

REFERENCES

1. Mossalaei, H. and K. Sarabandi, "Magneto-dielectrics in electromagnetics: Concept and applications," *IEEE Trans. Antennas and Propagation*, Vol. 52, No. 6, 1558–1567, 2004.
2. O'Brian, S. and J. B. Pendry, "Magnetic activity at infrared frequencies in structured photonic crystals," *J. of Physics: Condensed Matter*, Vol. 14, 6383–6394, 2002.
3. Schelkunoff, S. A. and H. T. Friis, *Antennas: Theory and Practice*, Ch. 19, J. Wiley & Sons, N.Y., 1952.
4. Tretyakov, S., *Analytical Modeling in Applied Electromagnetics*, Artech House, Norwood, MA, 2003.
5. Kostin, M. V. and V. V. Shevchenko, "Theory of artificial magnetic substances based on ring currents," *Sov. J. Communic. Technology and Electronics*, Vol. 38, 78–83, 1993.
6. Kostin, M. V. and V. V. Shevchenko, "Artificial magnetics based on double circular elements," *Proc. of Bianisotropics'94*, 49–56, Périgueux, France, 1994.
7. Mossalaei, H. and K. Sarabandi, "Embedded-circuit and RIS meta-substrates for novel antenna design," *2004 IEEE Antennas and Propagation Society International Symposium*, Vol. 1, 301–304, June 20–25, 2004.
8. Lindell, I. V., A. H. Sihvola, S. A. Tretyakov, and A. J. Viitanen, *Electromagnetic Waves in Chiral and Bi-Isotropic Media*, Artech House, Norwood, MA, 1994.
9. Serdyukov, A. N., I. V. Semchenko, S. A. Tretyakov, and A. Sihvola, *Electromagnetics of Bi-Anisotropic Materials: Theory and Applications*, Gordon and Breach Science Publishers, Amsterdam, 2001.
10. Lagarkov, A. N., V. N. Semenenko, V. A. Chistyayev, D. E. Ryabov, S. A. Tretyakov, and C. R. Simovski, "Resonance properties of bi-helix media at microwaves," *Electromagnetics*, Vol. 17, No. 3, 213–237, 1997.
11. Pendry, J. B., A. J. Holden, D. J. Robbins, and W. J. Stewart,

- “Magnetism from conductors and enhanced nonlinear phenomena,” *IEEE Transactions on Microwave Theory and Techniques*, Vol. 47, 2075–2084, 1999.
12. Marqués, R., F. Medina, and R. Rafi-El-Idrissi, “Role of bianisotropy in negative permeability and left-handed metamaterials,” *Physical Review B*, Vol. 65, 144440.
 13. Shamonina, E., V. Kalinin, K. Ringhofer, and L. Solymar, “Magneto-inductive waves in one, two and three dimensions,” *J. Appl. Phys.*, Vol. 92, No. 10, 6252–6261, 2002.
 14. Wiltshire, M. C. K., J. V. Hajnal, J. B. Pendry, and D. J. Edwards, “Near field imaging with magnetic wires,” *Optics Express*, Vol. 1, 709–715, 2003.
 15. Collin, R. E., *Foundations for Microwave Engineering*, 2nd ed., IEEE Press, New York, 2001.
 16. Sihvola, A., *Electromagnetic Mixing Formulas and Applications*, IEE Electromagnetic Waves Series 47, London, 1999.
 17. Ikonen, P., S. I. Maslovski, S. A. Tretyakov, and I. A. Kolmakov, “New artificial high-permeability material for microwave applications,” *Progress in Electromagnetics Research Symposium*, 485–488, Pisa, Italy, March 2004.

Stanislav Maslovski was born in Leningrad, USSR (now St. Petersburg, Russia) in 1975. He received the M.Sc. and the Candidate of Sciences (Ph.D.) degrees in radiophysics from the St. Petersburg State Polytechnical University in Russia in 1999 and 2004, respectively. Presently, he is with the Radio Laboratory of the Helsinki University of Technology in Finland. His main interests are within the electromagnetic metamaterial research, active materials, spatial dispersion phenomena, and antenna systems.

Pekka Ikonen was born on December 30, 1981, in Mäntyharju, Finland. He is currently studying towards the M.Sc. degree in communications engineering in the Helsinki University of Technology. From year 2002 he has been working as a research assistant in the Radio Laboratory, HUT. His current research interests include novel antennas utilizing artificial materials as well as high-permeability materials for microwave applications. Mr. Ikonen received the IEEE Antennas and Propagation Society Undergraduate Research Award for 2003–2004 and the IEEE Microwave Theory and Techniques Society Undergraduate/Pre-Graduate Scholarship for 2004–2005.

Igor Kolmakov was born in Abakan, Russia, in 1978. He received the B.Sc. degree (diploma with honour) from the St. Petersburg Electrotechnical University “LETI”, Russia, in 2000, the M.Sc. degree (diploma with honour) from the St. Petersburg Electrotechnical University “LETI”, Russia, in 2002, both in electrical engineering, and is currently working toward the Ph.D. degree in antennas and microwave engineering at the same university. From 2002 to 2003, he was a Teaching Assistant with the Department Microelectronics and Radio Engineering, St. Petersburg Electrotechnical University “LETI”. His research interests include electromagnetic simulation of microwave planar passive devices, microwave circuit design, antenna design, and metamaterials. Mr. Kolmakov was the recipient of the State Prize for young scientists for 2003 year. He is the recipient of the INTAS Young Scientist Fellowships 2003.

Sergei A. Tretyakov received the Dipl. Engineer-Physicist, the PhD, and the Doctor of Sciences degrees (all in radiophysics) from the St. Petersburg State Technical University (Russia), in 1980, 1987, and 1995, respectively. From 1980 to 2000 he was with the Radiophysics Department of the St. Petersburg State Technical University. Presently, he is professor of radio engineering in the Radio Laboratory, Helsinki University of Technology. His main scientific interests are electromagnetic field theory, complex media electromagnetics and microwave engineering. Prof. Tretyakov served as Chairman of the St. Petersburg IEEE ED/MTT/AP Chapter from 1995 to 1998.

Mikko Kaunisto was born in Finland, in 1963. He received the B.Sc. degree from University of Helsinki, in 2001. In 1992 he joined the Electronics Research Unit at the Department of Physical Sciences at University of Helsinki. Since 1995 he has been with the Information Technology Department at VTT Technical Research Centre of Finland. His research interest include Electromagnetic field simulations and PBG/EBG materials.